UDC 550.837:551.24(477)

Ľubomír KSEŇAK[1], Karol BARTOŠ[2], Katarína PUKANSKÁ[3], Kamil KYŠEĽA[4]

[1–4] Institute of Geodesy Cartography and GIS, Technical University of Košice, 19, Park Komenského Košice, 04200, Slovakia, tel. +421556022960; e-mail: [1] lubomir.ksenak@tuke.sk; [2] karol.bartos@tuke.sk; [3] katarina.pukanska@tuke.sk; [4] kamil.kysela@tuke.sk

https://doi.org/10.23939/jgd2023.01.005

SPATIO-TEMPORAL ANALYSIS OF SURFACE WATER EXTRACTION METHODS RELIABILITY USING COPERNICUS SATELLITE DATA

The aim of this research is the comparison and subsequent evaluation of the suitability of using SAR (Synthetic Aperture Radar) and multispectral (MSI) satellite data of the Copernicus program for mapping and accurate identification of surface water bodies. The paper considers sudden changes caused by significant climatological-meteorological influences in the country. The surface guidance extraction methodology includes the standard preprocessing of SAR images and concluding the determination of threshold values in binary mask generation. For MSI images, water masks are generated through automatic algorithmic processing on the Google Earth Engine cloud platform. During SAR image processing, it has been found that the VV polarization configuration type (vertical-vertical) is the most suitable. The Lee and Lee Sigma filters are recommended for eliminating radar noise. The chosen window size for filtering depends on the specific object and its spatial extent. The extraction of water surfaces from the MSI image is conducted using the Normalized Difference Water Index (NDWI), Modified Normalized Difference Water Index (MNDWI), a pair of Automated Water Extraction Index (AWEI) indices, and Water Ratio Index (WRI). Results are evaluated both graphically and numerically, using quantitative accuracy indicators to refine them. Automatic extraction of water surfaces from MSI images in the GEE platform environment is a fast, efficient, and relatively accurate tool for determining the true extent of groundwater. In conclusion, this research can provide more reliable estimates of hydrological changes and interannual variations in water bodies in the country. When combined with multitemporal monitoring, these results can be an effective tool for permanent monitoring of floods and droughts.

Key words: Remote Sensing; Surface Water; Synthetic Aperture Radar; Sentinel-1; MSI Images; Sentinel-2; Google Earth Engine.

Introduction

Water resources on our planet are of great *importance to the population and are irreplaceable* from the point of view of evaluating the climatic and ecological aspects of the country [Sekertekin, 2019]. Among the most important representatives of surface water are rivers, lakes, and water reservoirs with significant seasonal variations [Jiang et al., 2020]. Their shape and size changes [Zeleňáková et al., 2019] are primarily influenced by anthropogenic activity, climatic factors, and significant changes in meteorological conditions [Holgerson and Raymond, 2016]. Such changes can affect the environment, biodiversity, and the population's living conditions [Nilson et al., 2005]. The survey of surface water bodies and the definition of their spatial distribution has fundamental significance for water resources management and understanding of hydrological processes [Burshtynska et al., 2017].

Remote sensing techniques and the produced satellite images are helpful tools for evaluating the surface properties of the Earth and provide valuable information for water resources analysis [Burshtynska et al., 2019]. The relevant fact is that remote sensing data have a significant position in characterizing hydrological properties and conditions in different environments [Zhu and Abdelkareem, 2021]. The ability of SAR backscattered and emitted radiation to penetrate the atmosphere under any conditions, prefer this type of data for water surface monitoring. An important feature is the reflectivity of the surface, also known as the radar backscatter coefficient σ0. This coefficient is a function of surface parameters such as humidity, roughness, topography, and others, as well as radar system parameters such as angle of incidence, frequency, and polarization [Lee and Pottier, 2017]. Exactly the incidence angle of the radar signal and its size changes can produce deviations in the resulting backscatter values [Paluba et al., 2021]. To map water resources using SAR images, the application of not only cluster algorithms or different classification methods but also approaches such as manual determination of threshold values or their automatic segmentation using algorithms appears to be a suitable tool [Pulvirenti et al., 2013].

Monitoring the condition, extent, and quality of management has an irreplaceable position in water resources management [Gergeľová et al., 2023]. The

extraction of these features by remote sensing techniques from optical images is a very relevant part of detecting and understanding changes in the landscape [Hlotov and Biala, 2022]. Extraction methods of surface water bodies from multispectral images include classification (supervised and unsupervised), division of density bands, and the most popular approach, which is the calculation of spectral indices of water [Li et al., 2013]. This calculation method represents the transformation of the ratio of bands from a multispectral image with different spectral responses for individual land cover types [Sun et al., 2012]. This approach can be constantly considered an effective, reliable, and optimal tool, mainly due to the increase in differences between water and other bodies. Of course, using some indices in urbanized areas and with high albedo can lead to a results overestimation. Elimination of these effects, caused mainly by heterogeneous and mixed elements in the background, is through binary threshold segmentation. Currently, there are several approaches, such as the clustering methods, histogram methods, method of attribute similarity, and the most popular Otsu method.

It is possible to say that long-term multi-temporal monitoring using multiple data and multiple approaches has the potential to yield the most accurate characteristics of surface water bodies.

Purpose

The main goal of this research is to assess the suitability of using SAR and multispectral data to map surface water and for the most accurate identification of its extent. It focuses on changes in these formations due to recent climate-meteorological changes.

Study Area

The location of the Bodrog River (see Fig. 1) is in eastern Slovakia in the East Slovakian lowland. This river begins as the confluence of two rivers: the Ondava and the Latorica, near the Zemplín and the Svätá Mária municipalities. The flow of the Bodrog continues to the southwest towards Hungary. The length of the Bodrog River is 67 km, while the mouth of the Bodrog is in the Hungarian Tisa River, near Tokaj town. For the Bodrog basin, significant differentiated precipitation throughout the year is typical. Specifically, the highest annual rainfall precipitation of around 1,000 mm/year is typical for the Vihorlat mountains and their surroundings. Quite the opposite, some areas of East Slovak Lowland have the lowest total annual precipitation, with an approximate value of 550 mm/year. Regarding the hydrological conditions from December 2017 to February 2018, the rainfall precipitation was above the annual average – the same interval chosen for the research. The execution of this research is into three locations of the area of interest.

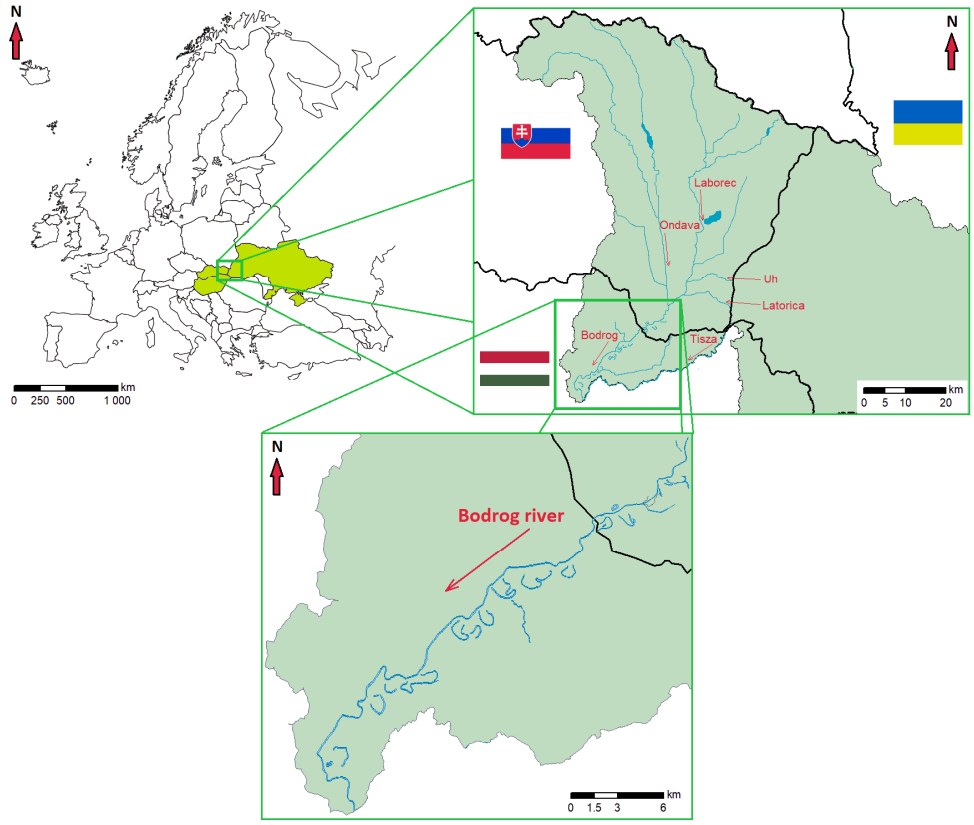

Fig. 1. Graphic interpretation of the geographical location of the study area.

Methodology

Extraction of water surfaces based on SAR images includes several steps of radar image pre-processing. Firstly, it is necessary to obtain information about the satellite's orbit. It is the so-called precise orbit ephemeris with information about its position and speed. This information is not included in the data product immediately after the acquisition process. For this step, the Apply Orbit File function is appropriate, which also allows us to obtain more accurate processing results thanks to the improvement of geocoding.

When working with SAR images, it is well-known that low-energy backscattered signals can result in point noise, particularly with cross-polarization channels. This type of noise, including thermal noise, is undesirable and can be eliminated using the Thermal Noise Removal tool. Additionally, changes in the Earth's curvature at the beginning of the area scanning can cause excessively increased noise values at the edges of the scene. For this reason, it is necessary to incorporate the so-called Border Noise Removal function into the SAR data pre-processing, especially when using entire scenes or edge parts.

Also, the relevant part of the pre-processing is the SAR image intensity recalculation to Sigma 0 values [Chen et al., 2020] using the calibration vector through the Radiometric Calibration function.

Another essential step is radar noise filtering to suppress the so-called Speckle Effect in the image. The speckle effect in SAR is caused by imaging coherent mechanisms that ensure the reflection of waves from many scatterers on the earth's surface [Ferro-Famil and Pottier, 2016]. It leads to an increased number of brighter and darker pixels, and the image layered in this way resembles pieces of salt and black pepper, the so-called Salt and Pepper effect [Liu et al., 2021]. this research compares several filtering tools that are now available.

The last step in the pre-processing of SAR GRD products is the application of Doppler terrain correction. In general, image SAR products have a specific geometric deformation of the image compared to the realistic geography and the influence of different weather conditions. For full-scale processing and evaluation of SAR data, it is necessary to eliminate or amend using geometric correction. Thus, geometric correction is a computational process of removing deformations to obtain a geographically consistent image. Its primary role is topographical distortion elimination using the DEM (Digital Elevation Model) and their subsequent transformation into the corresponding cartographic projection [Bayanudin and Jatmiko, 2016].

The next part of the methodology focuses on the water bodies extraction from the optical spectrum of remote sensing, that is, obtaining information through the spectral indices of water based on a mathematical principle. With the help of spectral bands with high spatial resolution, it is possible to gain relevant and timely information about water bodies with the required accuracy.

In general, two basic methods of water extraction are popular, the so-called single-band and multi-band methods. The first method is based on a specific band selection, while only a threshold value is defined to distinguish water from other surfaces. The second, the so-called multi-band principle, is a more effective method. In this case, the calculation method determines the ratio between two spectral bands. Thus, this ratio represents the region of the visible spectrum of electromagnetic radiation to near-infrared radiation. This research involves the application of several spectral indices of water. The most widely used index includes the Normalized Difference Water Index NDWI [McFeeters, 1996] for achieving the maximum reflectance of water using the green spectrum.

$$NDWI=\frac{(r_{Green}-r_{NIR})}{(r_{Green}+r_{NIR})}.$$

Another tool for determining water surfaces is the Modified Normalized Difference-Water Index MNDWI [Xu, 2006]. It uses visible green light and SWIR short-wave infrared radiation for calculation due to the more intense absorption of SWIR radiation compared to NIR.

$$MNDWI=\frac{(r_{Green}-r_{SWIR1})}{(r_{Green}+r_{SWIR1})}.$$

The subsequent benchmarked water extraction tool included in this study is the Automated Water Extraction Index. This indicator consists of two separate indices AWEInsh (not taking shadows) and AWEIsh (taking shadows). The dominance of this index is the effective elimination of non-water pixels, including dark built-up areas in urbanized areas [Feyisa et al., 2014].

$$AWE_{sh}I=r_{Blue}+2.5\times r_{Green}-$$
$$-1.5\times(r_{NIR}+r_{SWIR1})-0.25\times r_{SWIR2}.$$

Another indicator for water extraction is the WRI Water Ratio Index [Fang-fang et al., 2011; Shen and Li, 2010], which includes the application of four bands of spectral reflectance

$$WRI=\frac{(r_{Green}+r_{Red})}{(r_{NIR}+r_{SWIR1})}.$$

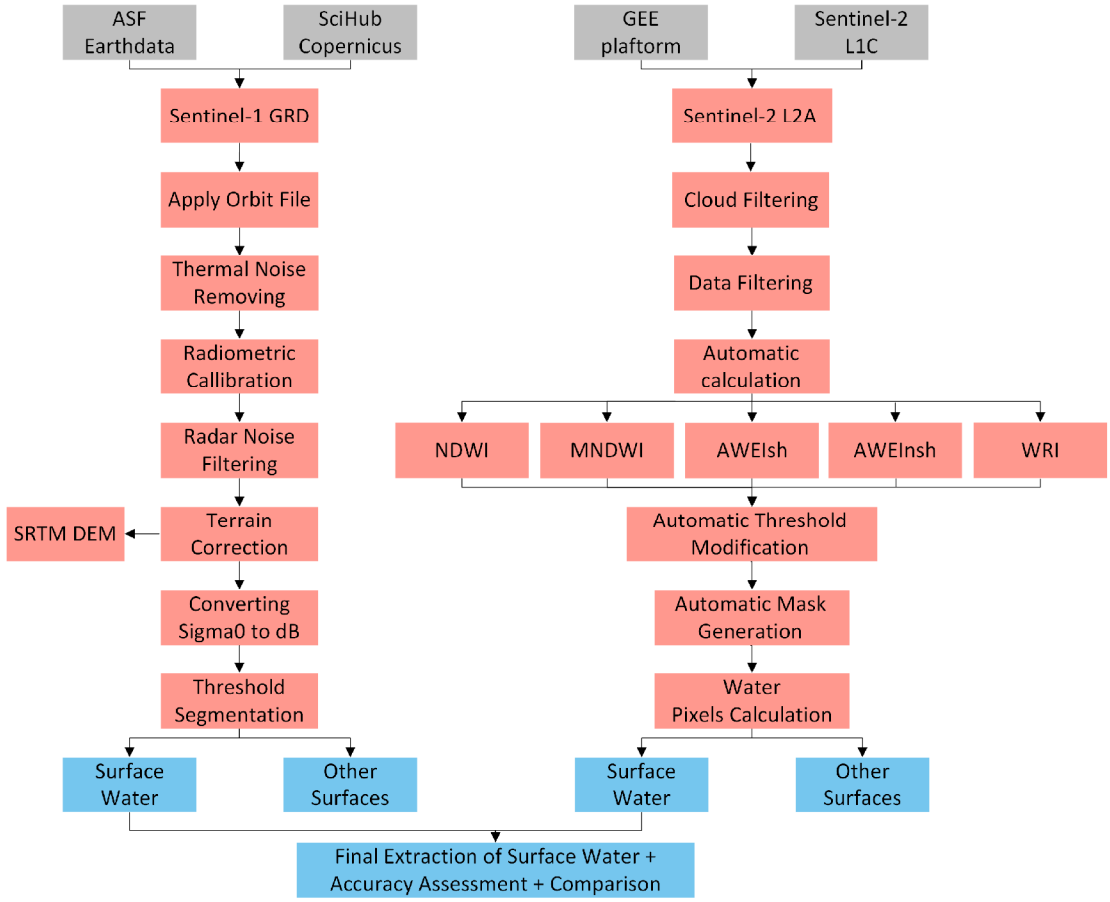

Fig. 2. Workflow of water bodies extraction using SAR and MSI data, including data preparation, pre-processing, data calculation, and results interpretation.

Data

Regarding the data structure, the Sentinel-1 mission represents satellites working in the radar part of electromagnetic radiation, especially using the C-band with a frequency of 5.405 GHz. Thanks to Synthetic Aperture Radar technologies is possible to obtain information about the earth's surface [Pakshyn et al., 2021] independently of the weather and lighting conditions on our planet. Currently, the Sentinel-1 mission consists only of the Sentinel-1A satellite. The flight anomaly of 23rd December 2021 caused the loss of data transmission from the Sentinel-1B satellite [Potin et al., 2022], while attempts to repair it were unsuccessful. This research includes using the Ground Range Detected GRD product-level data, which does not contain phase information. These are image products captured using the interferometric Wide Swath IW scanning mode. All images used in the research had a spatial resolution of 10 m × 10 m / pixel and both types of polarization configuration, i.e., VH and VV configuration.

Looking at the optical spectrum of Earth remote sensing, multispectral data with high spatial resolution represent a suitable type of data for documenting surface water changes [Pukanská et al., 2023]. For research purposes, freely available images of the Sentinel-2 satellite of the Copernicus program were used [Du et al., 2016]. Their preference over other available missions is mainly thanks to higher spatial and spectral resolution (see Table 1).

Table 1

Table of Sentinel-2 image bands with information about band resolution and wavelength

Band Type	Spatial Resolution, m	Central Wavelength, µm	Band Description
B1	60	0.443	Coastal aerosol
B2	10	0.490	Blue colour
B3	10	0.560	Green colour
B4	10	0.665	Red colour
B5	20	0.705	VNIR
B6	20	0.740	VNIR
B7	20	0.783	VNIR
B8	10	0.842	NIR
B8A	20	0.865	Narrow NIR
B9	60	0.945	Water Vapor
B10	60	1.380	SWIR-Cirrus
B11	20	1.610	SWIR
B12	20	2.190	SWIR

In the Sentinel-2 multispectral image processing, the authors used the L-2 data product level from the COPERNICUS/S2_SR collection in Google Earth Engine (GEE). This dataset includes images after atmospheric correction, terrain correction, and so-called cirrus correction (correction of thin-layer cloud type), processed using the Sen2cor program. The designed script includes the entire data processing process, including area definition of the spatial and temporal range of the images used, cloud filtering, calculation of water spectral indices with subsequent generation of binary masks, and numerical interpretation of the results.

Results

SAR Threshold Segmentation

The first part of the results consists of a comparison of SAR calibration threshold values. The conversion of obtained intensity values for each pixel was in the form of the backscattering coefficient. The expression of these values is in decibels (dB). For comparison, the analysis contains two types of images, i.e., the riverbed and its surroundings in a normal state (before the flood) and the river surroundings affected by the hydrological change (after the flood). Both polarization configurations, i.e., VV and VH, were used to compare the intensity. For this purpose, 25 control points were chosen on the surface near the river in the flood area. Evaluation of the pixel intensity was evaluated before the flood and during the flood. Also, the location of these control points was outside the vegetation areas. Specifically, it was to obtain the most optimal value of the intensity of the backscattered SAR signal. It was also about areas represented mainly by rough surfaces (e.g., agricultural land).

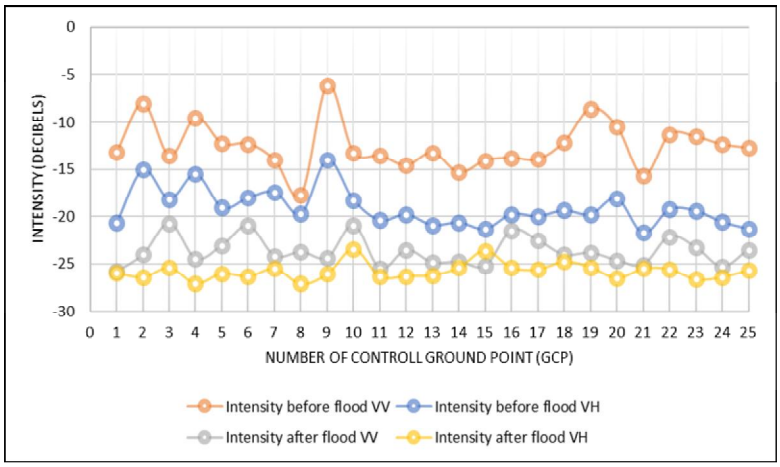

Fig. 3. The graphic comparison of the intensity of backscatter when using VV and VH polarization configuration concerning the interval before and after the flood.

The following graph (see Fig. 3) displays minimal differences between VV and VH polarization before and during flood activity, from −27 to −23 dB for VH polarization and from −26 to −20 dB for VV polarization. The intensity results show that among the factors influencing the results of VH polarization are mainly waterlogged soil due to long-lasting rains and melting snow. The results are also affected by the snow cover in the winter months (see Fig. 4).

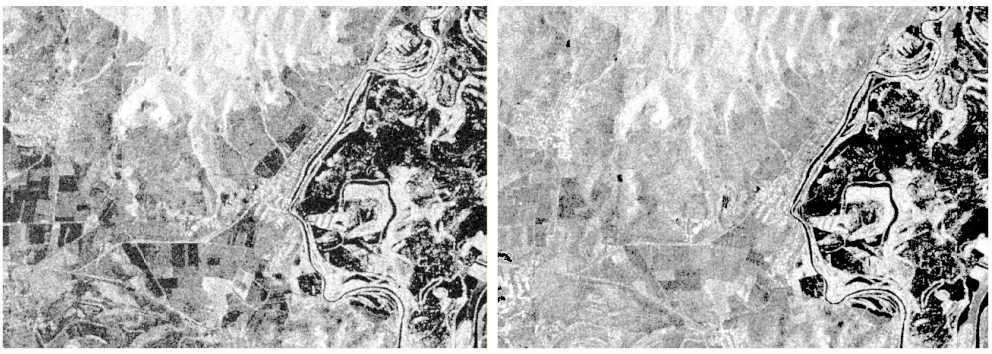

Fig. 4. Visual comparison of Sigma 0 intensity in dB for both types of polarization configuration, namely VH polarization on the left and VV polarization on the right.

Therefore, if we take a closer look at the mutual comparison of both types of polarization configurations, it is more appropriate to use VH polarization to monitor soil moisture. When using this polarization configuration, the results are affected by an increase in false positives, which was also confirmed by other researchers [Cao et al., 2019]. It is mainly due to cross-polarized images. It causes a slightly wide range of backscatter values, which causes incorrect classification of water bodies.

However, if we focus on open water surfaces, the VV polarization images show fewer incorrectly identified pixels of waterlogged soil than water surfaces, which was also confirmed by [Clement et al., 2017]. This effect verifies user accuracy results also (see Table 2). Lower backscatter values and their variability on smooth water surfaces are also substantial advantages.

Table 2

Table of comparison of accuracy assessment of water bodies extraction using VV and VH polarization

Month	Locality	Polarization Type	Producer Accuracy, %	User Accuracy, %	Kappa Coefficient
November 2017	L1	VV	72.1	80.1	0.718
		VH	76.9	79.4	0.721
	L2	VV	79.0	83.6	0.794
		VH	82.6	84.1	0.783
	L3	VV	80.7	88.1	0.851
		VH	84.6	89.3	0.849
January 2018	L1	VV	78.6	84.7	0.793
		VH	80.5	83.4	0.802
	L2	VV	81.3	89.5	0.846
		VH	87.1	84.7	0.851
	L3	VV	84.9	90.2	0.901
		VH	89.4	89.1	0.894
February 2018	L1	VV	77.4	85.7	0.789
		VH	79.6	78.3	0.737
	L2	VV	82.4	90.2	0.874
		VH	84.6	86.8	0.897
	L3	VV	84.9	93.1	0.917
		VH	88.3	87.4	0.899
March 2018	L1	VV	80.4	87.6	0.864
		VH	82.3	88.1	0.854
	L2	VV	86.4	91.4	0.891
		VH	86.9	90.5	0.907
	L3	VV	92.4	98.1	0.934
		VH	96.1	99.2	0.964
April 2018	L1	VV	80.4	86.1	0.849
		VH	82.7	87.4	0.854
	L2	VV	87.6	90.7	0.894
		VH	90.2	88.1	0.902
	L3	VV	89.5	95.4	0.931
		VH	91.3	93.1	0.928

Based on the achieved results, it is possible to say that VV polarization has a better potential to identify partially flooded formations, which is confirmed by [Manjusree et al., 2012]. This approach can be helpful in flood damage assessment. The interval in December 2017 was not included in the table (MSI processing was not successful in this interval as described in the chapters below).

Elimination of Radar Noise

Another part of the results focuses on the radar noise filtering from the image, specifically the assessment of the suitability of using several filtering tools for this purpose. Two types of SAR images were analyzed, i. e. after radar noise filtering (Lee filter with a window size of 3×3) and without filtering, for confirmation importance of noise elimination. For this procedure, the authors chose the specific territory of the site of interest 3. The results interpretation is in the form of binary masks.

The first results demonstrate that the filtered image contains a minimum of unwanted noisy pixels with high backscatter. Such an image can ensure continuity in the extraction of water surfaces. At the same time, there is an assumption of significant minimization of random noises outside water bodies.

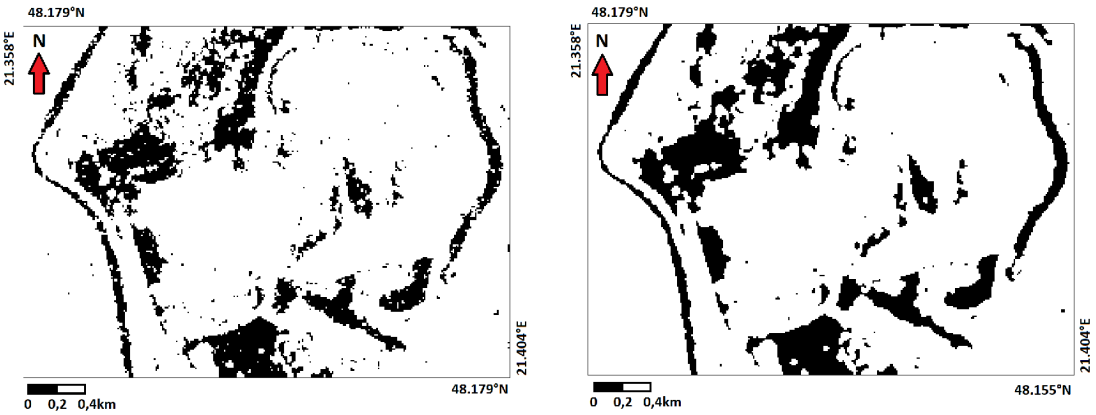

Fig. 5. An example of radar noise elimination in a selected area of interest in locality 3 using a Lee filter with a window size 3×3 (right) and a binary image without elimination (left).

Radar noise filtering was performed based on the above assumptions using several filtering tools. This research used the following types of filters:

- Lee filter.
- Lee Sigma filter.
- Refined Lee filter.
- Gamma MAP (Maximum a Posteriori) filter.
- and Median filter.

This comparison of filter tools produced some variation in the results. The Lee Sigma filter performed sufficient filtering of dark pixels. The Gamma MAP tool proves its dominance in the extensive water bodies mapping. The Refine Lee filter, in turn, brought a smoother texture to the resulting image. The Lee and the Median filter produced equally reliable results. These tools were also compared regarding the size of the used window (see Table 3).

It is clear from the results that the radar image without radar noise filtering contains a higher number of dark radar noise pixels, which evokes inaccuracies in the results. It follows that radar noise filtering plays a relevant role in eliminating errors in quantitative calculations (see Fig. 6).

If we look at the results, the window size dimensions 7×7 and larger are not applicable for mapping narrower riverbeds. The result is a set of incorrectly averaged pixels in the trough area due to the change in the spatial resolution of the image (the highest deviation values).

Based on the achieved numerical and graphical results, it is possible to conclude that the most suitable tools are Lee and Lee Sigma (possibly also Median). The dominance of the Lee filter is mainly the effective minimalization of non-water pixels.

Table 3

Table of the numerical comparison of speckle filter tools in the selected area in location 3 (grey cells represent the lowest value)

Filter Type	Window Size	Extend of Surface Water by Mask, km^2	Deviation from the Mean, %	Deviation from the Mean (3×3 and 5×5), %	Deviation from the Mean (3×3), %
Lee	3 × 3	1.337	4.89	1.19	0.53
	5 × 5	1.388	8.93	5.09	4.40
	7 × 7	0.977	–23.34	–26.04	–26.52
Lee Sigma	5 × 5	1.278	0.27	–3.26	–3.90
	7 × 7	1.074	–15.76	–18.72	–19.26
Refined Lee	–	1.447	13.55	9.55	8.83
Gamma MAP	3 × 3	1.348	5.75	2.03	1.36
	5 × 5	1.178	–7.60	–10.85	–11.44
Median	3 × 3	1.305	2.36	–1.24	–1.89
	5 × 5	1.414	10.95	7.04	6.34
No filter	–	1.582	24.16	19.79	19.00

The results in the above table (see Table 3.) confirm the suitability of using windows with dimensions 3×3 or 5×5. In the case of narrower waterways, such as the Bodrog River, a 5×5 window usage is less suitable due to the decreasing width of the riverbed. In the case of a flood-free interval (November 2017), this causes significant inaccuracies in the results. For this reason, filtering with a Lee filter with a window size of 3×3 was used for all three localities of interest.

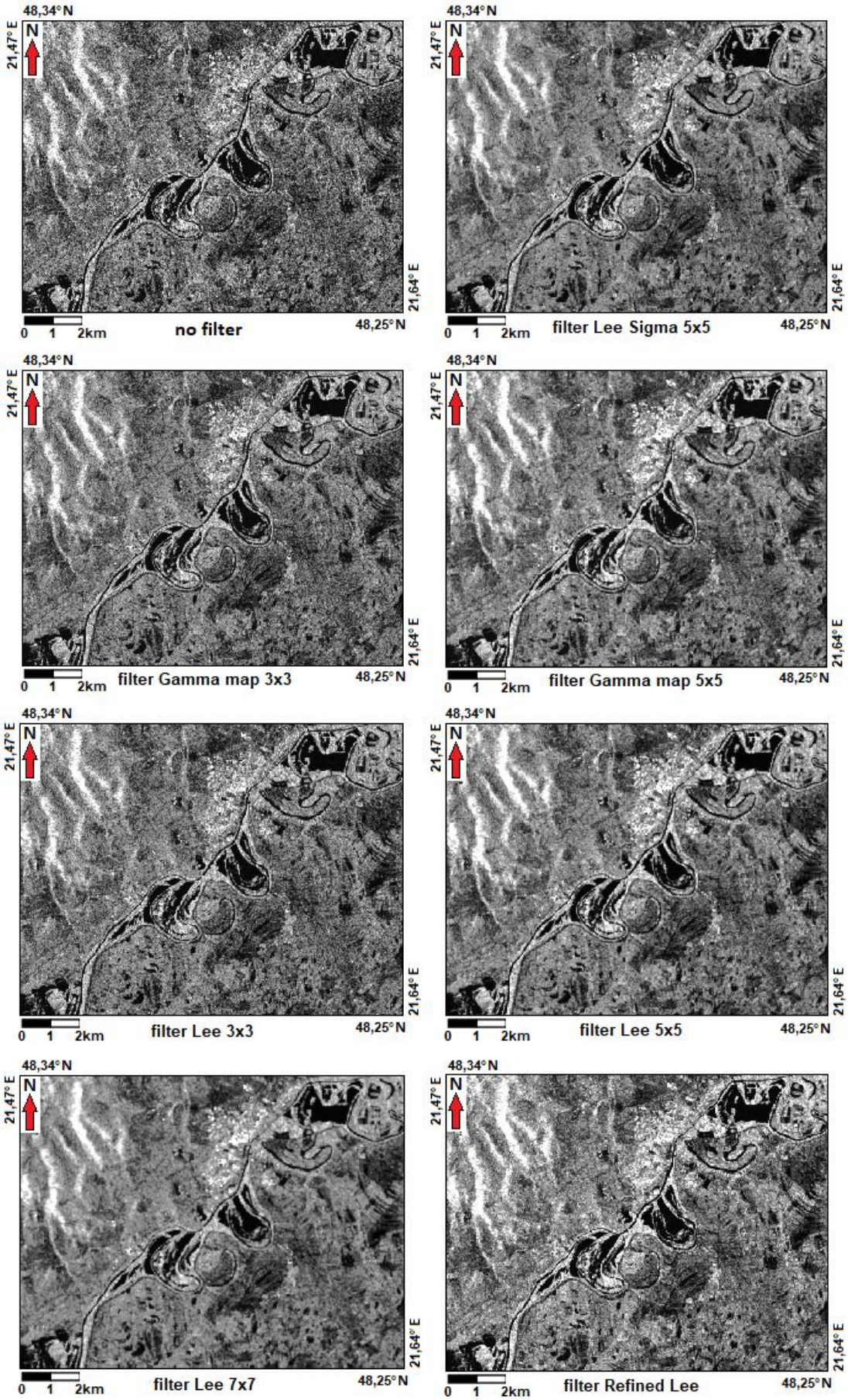

Fig. 6. A sample comparison of radar noise filtering results for selected filtering tools.

Water extraction by spectral indices

For the comparison of mathematical indicators for the water bodies determination, it was appropriate to find areas of interest with the representation of standing water bodies (e. g. dead river arm, flooded arable land, and others) and a flowing river. It was also necessary to consider the immediate surroundings in terms of the occurrence of high albedo areas, shady places, and urbanized areas. Of course, the extraction comparison was carried out over a flowing river and stagnant water in a death bed also, partially covered by low vegetation (see Fig. 7).

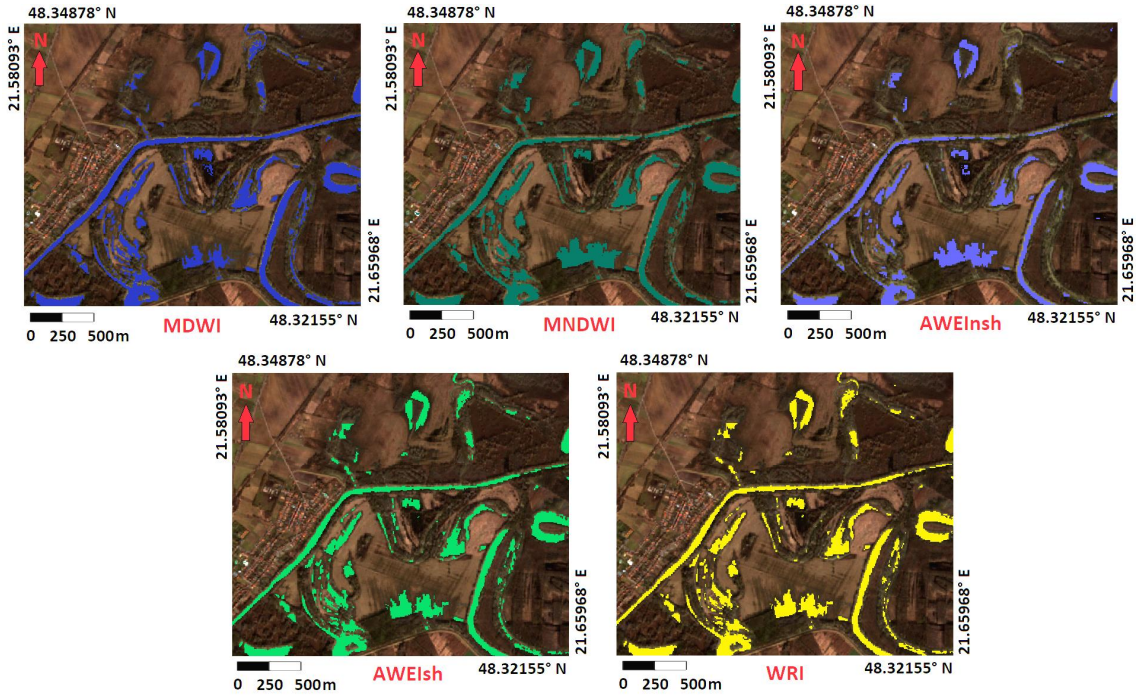

Fig. 7. The image of a comparison of automated water bodies extraction using NDWI, MNDWI, AWEInsh, AWEIsh, and WRI spectral indices.

The results of the mutual comparison show an increase in the separation of water surfaces from other non-water features of the landscape. It is clear from obtained values that the underestimated results are significant for the AWEInsh index. That is probably due to the presence of shadows in the images. If we look at water body extraction using the NDWI and MNDWI water index, we can see little differences in a few tens of square meters. This phenomenon is the same for other compared images in another temporal interval, likewise in localities 2 and 3. Regarding the MNDWI index, its main drawback is its implementation in urban areas with high albedo. The same is true for the AWEIsh indicator. This phenomenon is due to smaller negative values with more SWIR light reflection than green light (i. e. classes such as soil, vegetation, and urbanized area).

If we look at the numerical calculation of the area of water bodies, in this comparison, water areas in the range from 0.65 to 0.99 km^2 were achieved (see Table 4). However, if we do not include extraction using the AWEInsh index in the comparison, the resulting area represents an interval with a maximum difference of 0.055 km^2, or 5.5 hectares. Thus, the resulting percentage deviations from the mean value range from – 1.8 % (AWEIsh) to – 3.22 % (WRI).

Table 4

Table of the numerical comparison of water masks area in specific territory

Spectral Index	Water Bodies Extend [km^2]	Deviation from the Mean (without AWEInsh), km^2	Deviation percentile, %
NDWI	0.991837	0.023	2.30
MNDWI	0.993920	0.025	2.51
AWEInsh	0.652598	–0.316	–48.48
AWEIsh	0.951516	–0.017	–1.84
WRI	0.938675	–0.030	–3.23

The entire process of comparing the results of the extraction of water bodies is obtained through the automatic segmentation of threshold values through the algorithm in the Google Earth Engine platform. The User Accuracy and Producer Accuracy values were comparable to the same accuracy indicators in the SAR image processing.

Discussion

As for evaluating the pros and cons of using Sentinel-1 SAR imagery, the positives include that almost all images are suitable for water extraction. That is, regardless of weather and weather conditions. These data are appropriate for mapping surface water bodies (without significant surface wave presence) thanks to the strong backscatter contrast at water surfaces. Elimination and correction of these effects can be implemented using geometric and radiometric correction) and SAR noise filtering is also relevant. From the presented results, it follows that the using of VV polarization has a significant effect on the backscatter values in water surfaces with vegetation presence, which is also confirmed by this study [Tsyganskaya et al., 2018]. If we consider the radar noise, its elimination using the Lee tool with a 3×3 window size appears to be the most suitable tool in this study, which is also confirmed by this research [Notti et al., 2018]. Of course, for larger water bodies, it is advisable to use a 5×5 window size, or even the Lee Sigma tool, which indicates the resulting deviations also. The segmentation of threshold values in the binary mask generation by Otsu's principle represents a suitable way of interpreting the results even in the present.

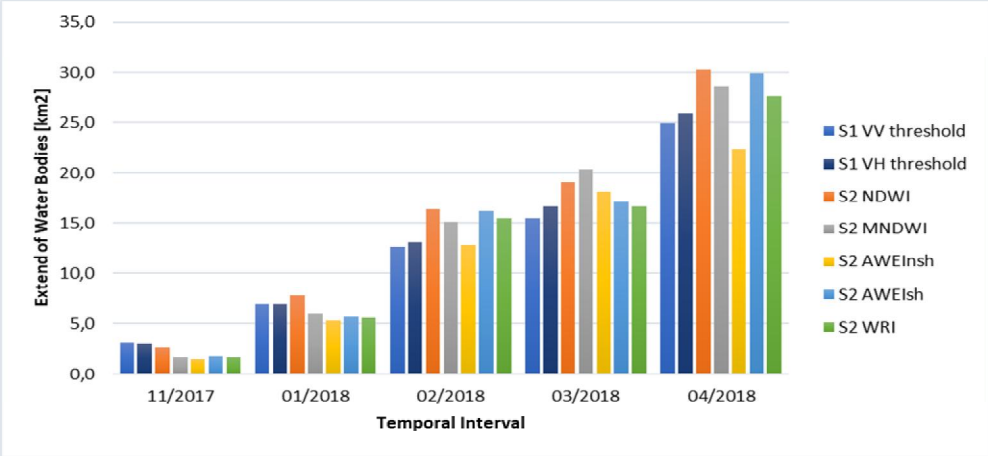

Fig. 8. The graph of spatial numerical evaluation of changes in the extent of water areas in locality 3.

The mapping of water bodies using SAR images also has certain imperfections. The first is to blend multiple pixels near riverbanks when extracting water masks. This so-called phenomenon – volume scattering, is conditioned by the wider variability of backscattering near vegetation precisely at VH polarization. Thus, it is possible to say that the vegetation present in the marginal parts of water bodies can cause inaccuracies in the results.

As for the Sentinel-2 MSI data characterization, using these data for water extraction has several drawbacks. The most significant is the presence of clouds. Specifically, in the 12/2017 period, all available images contained an excessive cloud cover. Due to subsequent insufficient cloud filtering, these data products were excluded (see Fig. 9). Even more, locality 1 was excluded from the resulting comparison due to the lack of cloud-free data products, i. e. even after cloud filtering.

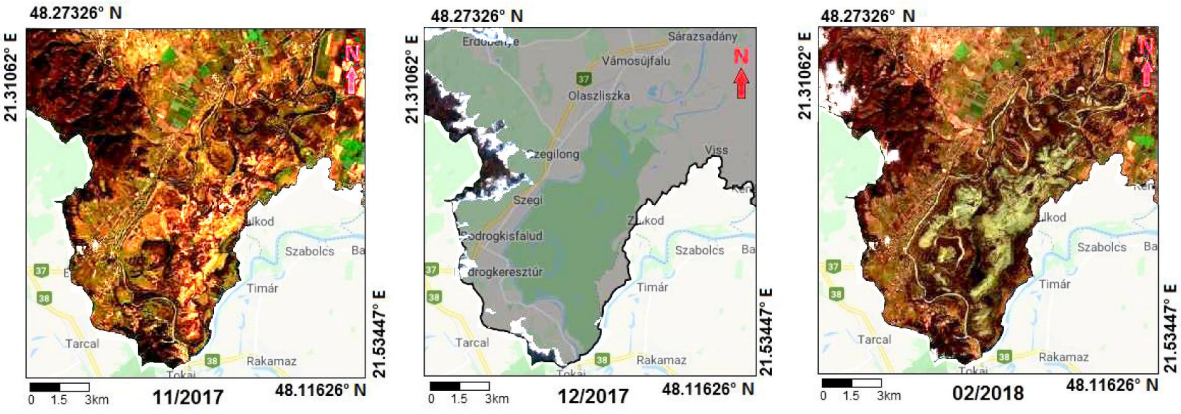

Fig. 9. The cloud filtration errors in the temporal interval 12/2017 in comparison to other images.

If we look at the results, increasing noise values due to image processing has a substantial accuracy impact. An appropriate step, therefore, seems to be the comparison of several spectral indices for water extraction and their results for the site of interest. Other disadvantages include the reflectivity of the signal from the bottom in areas of shallow-stagnant water [Tsyganskaya et al., 2019]. Thus, this phenomenon can significantly influence the results.

From the presented results and their comparison, among the biggest advantages of using Sentinel-2 images is the better spatial resolution of the final water masks. It is a prerequisite for a more coherent final appearance of the water flow mask and its channel, which is also confirmed by [Zhang et al., 2020]. Also, the results show a better ability to detect the signal in riverbank areas.

Originality

The automatic extraction of water surfaces from multispectral imagery in the GEE platform environment is a relatively accurate, fast, and efficient tool for determining the true extent of groundwater in the landscape.

Practical significance

The results of this research will make it possible to reliably estimate sudden hydrological changes in the country due to extreme floods and droughts, which could harm land use.

Conclusions

To assess the reliability of the extraction of surface lead formations, it is possible to say that all penetrations have their strengths and weaknesses. A strong domain of Sentinel-2 multispectral images is their minimal influence by noise (radar, random, thermal, and others). Thanks to the wider diversity of spectral indices of water, it is possible to obtain more accurate results, respectively, it is easier to detect random errors and mistakes during water extraction. In the future, the authors would also like to focus on the use of satellite data from third-party missions with a higher spatial resolution (Pleiades, Spot).

Regarding the segmentation of the threshold values, it can be stated that the added noise elimination could cause a slight improvement in the validity of the achieved results. For further refinement, the application of using multiple threshold segmentation approaches in the binary mask generation process could be helpful. An automatic algorithmic processing approach in the Google Earth Engine environment appears to be a suitable tool. This method produced more reliable results than the manual determination of threshold values.

When considering the SAR images utilized, employing commercial satellite data with a greater spatial resolution may prove advantageous.In further research, the authors would like to focus on GAN (Generative Adversarial Network) application to improve the spatial resolution of the image. So is the application of the SAM (Segment Anything Model) approach.

However, the influence of the ascending and descending orbit of the satellite on the accuracy of water extraction can be observed in the SAR GRD extraction results. To refine the results, it is possible to incorporate information from ascending and descending dual-polarized images combined with polarimetric components, such as the so-called SPAN, DI, and PR. If we are talking about setting threshold values, the independent approach could improve the results, e. g. Double-window Flexible Pace Search access method.

It is clear from the presented results that the continuous improvement of existing and the search for new approaches to water extraction is essential in the current climate-prone time.

Acknowledgements

The study is the result of Grant Projects of the Slovak Ministry of Education of the Slovak Republic VEGA 1/0340/22, and KEGA 3TUKE-4/2023.

References

Bayanudin, A. A., & Jatmiko, R. H. (Eds.). (2016). Orthorectification of Sentinel-1 SAR (synthetic aperture radar) data in Some parts of south-eastern Sulawesi using Sentinel-1 toolbox. *In IOP Conference Series: Earth and Environmental Science* (Vol. 47, No. 1, p. 012007). IOP Publishing.

Burshtynska, Kh. V., Babushka, A. V., Bubniak, I. M., Babiy, L. V., & Tretyak, S. K. (2019). Influence of geological structures on the nature of riverbed displacements for the rivers of the Dnister basin upper part. *Geodynamics*, *2*(27), 24–38. https://doi.org/10.23939/jgd2019.02.024

Burshtynska, Kh. V., Tretyak, S., & Halockin, M. (2017). Study of horizontal displacements of the channel of Dniester river using remote sensing data and GIS-technologies. *Geodynamics*, *2*(23), 14–24. https://doi.org/10.23939/jgd2017.02.014 (in Ukrainian)

Cao, H., Zhang, H., Wang, C., & Zhang, B. (2019). Operational flood detection using sentinel-1 SAR data over large areas. *Water*, *11*(4), 786. https://doi.org/10.3390/w11040786

Chen, F., Chen, X., Van de Voorde, T., Roberts, D., Jiang, H., & Xu, W. (2020). Open water detection

in urban environments using high spatial resolution remote sensing imagery. *Remote Sensing of Environment, 242,* 111706. https://doi.org/10.1016/j.rse.2020.111706

Clement, M. A., Kilsby, C. G., & Moore, P. (2017). Multi-temporal synthetic aperture radar flood mapping using change detection. *Journal of Flood Risk Management, 11*(2), 152–168. https://doi.org/10.1111/jfr3.12303

Du, Y., Zhang, Y., Ling, F., Wang, Q., Li, W., & Li, X. (2016). Water bodies' mapping from sentinel-2 imagery with modified normalized difference water index at 10-m spatial resolution produced by sharpening the Swir Band. *Remote Sensing, 8*(4), 354. https://doi.org/10.3390/rs8040354

Fang-fang, Z., Bing, Z., Jun-sheng, L., Qian, S., Yuanfeng, W., & Yang, S. (2011). Comparative analysis of automatic water identification method based on multispectral remote sensing. *Procedia Environmental Sciences, 11*, 1482–1487. https://doi.org/10.1016/j.proenv.2011.12.223

Ferro-Famil, L., & Pottier, E. (2016). *1 - Synthetic Aperture Radar Imaging. Microwave Remote Sensing of Land Surface.* Elsevier. pp. 1–65. ISBN 9781785481598 https://doi.org/10.1016/B978-1-78548-159-8.50001-3

Feyisa, G. L., Meilby, H., Fensholt, R., & Proud, S. R. (2014). Automated Water Extraction Index: A new technique for surface water mapping using landsat imagery. *Remote Sensing of Environment, 140*, 23–35. https://doi.org/10.1016/j.rse.2013.08.029

Gergelova, M. B., Kovanič, L., Abd-Elhamid, H. F., Cornak, A., Garaj, M., & Hilbert, R. (2023). Evaluation of spatial landscape changes for the period from 1998 to 2021 caused by extreme flood events in the Hornád Basin in eastern Slovakia. *Land, 12*(2), 405. https://doi.org/10.3390/land12020405

Hlotov, V., & Biala, M. (2022). Spatial-temporal geodynamics monitoring of land use and land cover changes in Stebnyk, Ukraine based on Earth remote sensing data. *Geodynamics, 1*(32), 5–15. https://doi.org/10.23939/jgd2022.02.005

Holgerson, M. A., & Raymond, P. A. (2016). Large contribution to inland water CO2 and CH4 emissions from very small ponds. Nature *Geoscience, 9*(3), 222–226. https://doi.org/10.1038/ngeo2654

Jiang, W., He, G., Pang, Z., Guo, H., Long, T., & Ni, Y. (2019). Surface water map of China for 2015 (SWMC-2015) derived from Landsat 8 satellite imagery. *Remote Sensing Letters, 11*(3), 265–273. https://doi.org/10.1080/2150704x.2019.1708501

Lee, J.S., & Pottier, E. (2017). *Polarimetric Radar Imaging* (1st ed.). CRC Press, Taylor & Francis Group: Boca Raton, FL, USA. https://doi.org/10.1201/9781420054989

Li, W., Du, Z., Ling, F., Zhou, D., Wang, H., Gui, Y., Sun, B., & Zhang, X. (2013). A comparison of land surface water mapping using the Normalized Difference Water Index from Tm, ETM+ and Ali. *Remote Sensing, 5*(11), 5530–5549. https://doi.org/10.3390/rs5115530

Liu, S., Gao, L., Lei, Y., Wang, M., Hu, Q., Ma, X., & Zhang, Y.D. (2021). SAR speckle removal using hybrid frequency modulations. *IEEE Transactions on Geoscience and Remote Sensing, 59*(5), 3956–3966. https://doi.org/10.1109/tgrs.2020.3014130

Manjusree, P., Prasanna Kumar, L., Bhatt, C. M., Rao, G. S., & Bhanumurthy, V. (2012). Optimization of threshold ranges for rapid flood inundation mapping by evaluating backscatter profiles of high incidence angle SAR images. *International Journal of Disaster Risk Science, 3*(2), 113–122. https://doi.org/10.1007/s13753-012-0011-5

McFeeters, S. K. (1996). The use of the normalized difference water index (NDWI) in the delineation of open water features. *International Journal of Remote Sensing,* 17(7), 1425–1432. https://doi.org/10.1080/01431169608948714

Nilsson, C., Reidy, C. A., Dynesius, M., & Revenga, C. (2005). Fragmentation and flow regulation of the world's large river systems. *Science, 308*(5720), 405–408. https://doi.org/10.1126/science.1107887

Notti, D., Giordan, D., Caló, F., Pepe, A., Zucca, F., & Galve, J. (2018). Potential and limitations of open satellite data for flood mapping. *Remote Sensing, 10*(11), 1673. https://doi.org/10.3390/rs10111673

Pakshyn, M., Liaska, I., Kablak, N., & Yaremko, H. (2021). Investigation of the mining departments influence of Solotvynsky salt mine SE on the Earth surface, buildings and constructions using satelite radar monitoring. *Geodynamics, 2*(31), 41–52. https://doi.org/10.23939/jgd2021.02.041

Paluba, D., Laštovička, J., Mouratidis, A., & Štych, P. (2021). Land cover-specific local incidence angle correction: A method for time-series analysis of forest ecosystems. *Remote Sensing, 13*(9), 1743. https://doi.org/10.3390/rs13091743

Potin, P., Colin, O., Pinheiro, M., Rosich, B., O'Connell, A., Ormston, T., ... & Torres, R. (Eds.). (2022). Status and Evolution of the Sentinel-1 mission. In IGARSS 2022-2022 *IEEE International Geoscience and Remote Sensing Symposium,* 4707–4710. IEEE.

Pukanská, K., Bartoš, K., Bakoň, M., Papčo, J., Kubica, L., Barlák, J., Rovňák, M., Kseňak, Ľ., Zelenakova, M., Savchyn, I., & Perissin, D. (2023). Multi-sensor and multi-temporal approach in monitoring of deformation zone with permanent monitoring solution and management of

environmental changes: A case study of solotvyno salt mine, Ukraine. *Frontiers in Earth Science, 11*. https://doi.org/10.3389/feart.2023.1167672

Pulvirenti, L., Pierdicca, N., Chini, M., & Guerriero, L. (2013). Monitoring flood evolution in vegetated areas using COSMO-SkyMed data: The Tuscany 2009 case study. *IEEE Journal of Selected Topics in Applied Earth Observations and Remote Sensing, 6*(4), 1807–1816. doi: 10.1109/JSTARS.2012.2219509.

Sekertekin, A. (2020). A survey on global thresholding methods for mapping open water body using sentinel-2 satellite imagery and Normalized Difference Water Index. *Archives of Computational Methods in Engineering, 28*(3), 1335–1347. https://doi.org/10.1007/s11831-020-09416-2

Shen, L., & Li, C. (Eds.). (2010). Water Body Extraction from Landsat ETM+ Imagery Using Adaboost Algorithm. *Proceedings of 18th International Conference on Geoinformatics*. Beijing, China: IEEE.

Sun, F., Sun, W., Chen, J., & Gong, P. (2012). Comparison and improvement of methods for identifying waterbodies in remotely sensed imagery. *International Journal of Remote Sensing, 33*(21), 6854–6875. https://doi.org/10.1080/01431161.2012.692829

Tsyganskaya, V., Martinis, S., Marzahn, P., & Ludwig, R. (2018). Detection of temporary flooded vegetation using Sentinel-1 time series data. *Remote Sensing, 10*(8), 1286. https://doi.org/10.3390/rs10081286

Tsyganskaya, V., Martinis, S., & Marzahn, P. (2019). Flood monitoring in vegetated areas using multitemporal sentinel-1 data: Impact of time series features. *Water, 11*(9), 1938. https://doi.org/10.3390/w11091938

Xu, H. (2006). Modification of normalised difference water index (NDWI) to enhance open water features in remotely sensed imagery. *International Journal of Remote Sensing, 27*(14), 3025–3033. https://doi.org/10.1080/01431160600589179

Zeleňáková, M., Fijko, R., Labant, S., Weiss, E., Markovič, G., & Weiss, R. (2019). Flood risk modelling of the SLATVINEC stream in Kružlov Village, Slovakia. *Journal of Cleaner Production, 212*, 109–118. https://doi.org/10.1016/j.jclepro.2018.12.008

Zhang, M., Chen, F., Liang, D., Tian, B., & Yang, A. (2020). Use of sentinel-1 GRD SAR images to delineate flood extent in Pakistan. *Sustainability, 12*(14), 5784. https://doi.org/10.3390/su12145784

Zhu, Q., & Abdelkareem, M. (2021). Mapping groundwater potential zones using a knowledge-driven approach and GIS analysis. *Water, 13*(5), 579. https://doi.org/10.3390/w13050579

Любомир КСЕНАК[1], Кароль БАРТОШ[2], Катаріна ПУКАНСЬКА[3], Каміль КІШЕЛЯ[4]

[1–4] Інститут геодезії, картографії та ГІС, Кошицький технічний університет, Парк Коменського, 19, Кошице, 04200, Словаччина, тел. +421556022960, e-mail: [1] lubomir.ksenak@tuke.sk; [2] karol.bartos@tuke.sk; [3] katarina.pukanska@tuke.sk; [4] kamil.kysela@tuke.sk

ПРОСТОРОВО-ЧАСОВИЙ АНАЛІЗ НАДІЙНОСТІ МЕТОДІВ ВИОКРЕМЛЕННЯ ПОВЕРХНЕВОЇ ВОДИ ЗА ДАНИМИ СУПУТНИКА COPERNICUS

Метою цього дослідження є порівняння та подальша оцінка придатності використання SAR (радара із синтетичною апертурою) та мультиспектральних (MSI) супутникових даних програми Copernicus для картографування та точної ідентифікації поверхневих водних тіл, враховуючи раптові зміни, спричинені значними кліматичними впливами**.** Методологія виділення наземних навігацій передбачає стандартну попередню обробку зображень SAR і завершення визначення порогових значень у генерації бінарної маски. Опрацювання зображень MSI охоплює автоматичну алгоритмічну обробку та подальшу генерацію водяних масок через хмарну платформу Google Earth Engine. Результати опрацювання зображення SAR показують, що тип конфігурації поляризації VV (вертикальна–-вертикальна) є відповідним типом поляризації. Якщо брати інструменти фільтрації

для видалення радіолокаційних шумів, то для цієї мети найкраще підходять фільтри Lee і Lee Sigma. Використовуваний розмір вікна залежить від конкретного типу об’єкта, а також від його просторового розміру. Екстракція водних поверхонь із зображення MSI обробляється за допомогою нормалізованого індексу різниці води (NDWI), модифікованого нормалізованого індексу різниці води (MNDWI), пари індексів автоматичного індексу вилучення води (AWEI) та індексу співвідношення води (WRI). Оцінка отриманих значень вилучення – графічна та числення – для уточнення результатів (з використанням кількісних показників точності). Автоматичне виділення водних поверхонь із зображень MSI у середовищі платформи GEE є порівняно точним, швидким і ефективним інструментом для визначення справжнього рівня ґрунтових вод. Підсумовуючи, можна сказати, що результати цих досліджень дають змогу достовірніше оцінювати раптові гідрологічні зміни, спричинені міжрічними коливаннями водойм країни. У поєднанні з різночасовим моніторингом цих змін вони можуть бути ефективним інструментом постійного моніторингу повеней і посух.

Ключові слова: ДЗЗ; поверхневі води; радар із синтетичною апертурою; Sentinel-1; зображення MSI; Sentinel-2; Google Earth Engine.

Received 12.04.2023